PCCP

RSC Publishing

PAPER

View Article Online
View Journal | View Issue

Cite this: *Phys. Chem. Chem. Phys.*, 2013, **15**, 4041

Fabrication and photoelectrochemical properties of ZnS/Au/TiO_2 nanotube array films†

Yan-Feng Zhu, Juan Zhang, Lu Xu, Ya Guo, Xiao-Ping Wang, Rong-Gui Du* and Chang-Jian Lin

Received 10th October 2012,
Accepted 21st January 2013

DOI: 10.1039/c3cp43572e

www.rsc.org/pccp

A highly ordered TiO_2 nanotube array film was fabricated by an anodic oxidation method. The film was modified by Au nanoparticles (NPs) formed by a deposition–precipitation technique and was covered with a thin ZnS shell prepared by a successive ionic layer adsorption and reaction (SILAR) method. The photoelectrochemical properties of the prepared ZnS/Au/TiO_2 composite film were evaluated by incident photon-to-current conversion efficiency (IPCE), and photopotential and electrochemical impedance spectroscopy (EIS) measurements under white light illumination. The results indicated that the Au NPs could expand the light sensitivity range of the film and suppress the electron–hole recombination, and the ZnS shell could inhibit the leakage of photogenerated electrons from the surface of Au NPs to the ZnS/electrolyte interface. When the 403 stainless steel in a 0.5 M NaCl solution was coupled to the ZnS/Au/TiO_2 nanotube film photoanode under illumination, its potential decreased by 400 mV, showing that the composite film had a better photocathodic protection effect on the steel than that of a pure TiO_2 nanotube film.

1 Introduction

Following the discovery of carbon nanotubes,[1] one dimensional (1D) materials and nanomaterials have attracted great interest in the academic world because of their geometrical morphologies and potential applications in nanoscale optical and electric devices.[2–8] Among the various 1D nanomaterials, the TiO_2 nanotube array film with a high ratio surface area and precisely controlled morphology, formed by electrochemical anodization, is expected to have potential applications in environmental purification,[9,10] water photolysis,[11,12] photovoltaic cells,[13,14] biomedical devices,[15,16] photocathodic protection,[17] and gas sensors[18,19] due to its non-toxicity, good chemical stability and outstanding electronic properties. However, there are some serious problems for TiO_2 applications. One of the major limitations of achieving high photoelectric conversion efficiency of TiO_2 is the fast recombination of the photoinduced charge carriers. To solve this problem, a rapid transfer of the charge carriers to prevent the electron–hole pairs from recombination is usually required. Decorating TiO_2 with noble metals can greatly enhance the surface activity due to the rapid transfer of photoelectrons, which can decrease the recombination with photoholes.[20,21] Recently, highly dispersed Au NPs supported on TiO_2 surfaces have become a focal point in some relevant investigations because of the reduction of electron–hole recombination in Au–TiO_2 composites.

Up to now, the Au–TiO_2 composite has been prepared by both physical and chemical methods, including the RF-sputtering approach,[22] sol–gel technique,[23] deposition–precipitation,[24] and photoreduction.[25] To prepare Au–TiO_2 nanotube films, first, the precursor ions ($AuCl_4^-$) must be transferred into the tubes through adsorption, ion-exchange, or ultrasonication; then, the precursors can be reduced by the electrochemical deposition,[26] UV irradiation,[27] sputtering,[28] or other methods.[29] It is vital to promote the dispersion of Au NPs in the preparation of a Au–TiO_2 composite film because its photoactivity is highly dependent on the shape, size, distribution and chemical states of Au NPs.[30] It is reported that Au NPs can effectively facilitate charge transport in the Au–TiO_2 composite film and improve the charge separation efficiency.[31] However, there are no reports related to the photocathodic protection effect based on Au modified-TiO_2 films.

ZnS is a stable semiconductor material with a wide band gap E_g = 3.8 eV, and it can also form a potential barrier at the electrode–electrolyte interface due to its more negative conduction band (−1.85 V *vs.* NHE)[32] than the Fermi level (+0.5 V *vs.* NHE)

State Key Laboratory of Physical Chemistry of Solid Surfaces, Department of Chemistry, College of Chemistry and Chemical Engineering, Xiamen University, Xiamen 361005, P. R. China. E-mail: rgdu@xmu.edu.cn; Tel: +86 592 2189192

† Electronic supplementary information (ESI) available. See DOI: 10.1039/c3cp43572e

of Au.[33] Consequently, the leakage of electrons from the Au surface to the film/electrolyte interface can be suppressed if the Au–TiO_2 composite film is covered by a ZnS shell, and a highly effective photocathodic protection property of the composite film can be obtained.

In the present work, we assembled highly dispersed Au NPs on the interior and exterior surfaces of the TiO_2 nanotubes synthesized by an anodization technique, and ZnS nanoparticles were prepared on the nanobube film by a successive ionic layer adsorption and reaction (SILAR) method to improve the photoelectrochemical effect of the film. We found that the ZnS/Au/TiO_2 composite film as a photoanode could provide a great photocathodic protection effect for 403 stainless steel (403SS).

2 Experimental

2.1 Preparation of ZnS/Au/TiO_2 nanotube array films

Ti foils (0.1 mm thickness, 99.7% purity) with dimensions of 15 × 10 × 0.1 mm were degreased by ultrasonic cleaning successively in acetone, ethanol, and deionized water, followed by rinsing with deionized water and drying at room temperature. TiO_2 nanotube array films were prepared on Ti foils by an anodization method in a 0.5 wt% HF solution under 20 V for 30 min in a two-electrode system with the Ti foil as the working electrode and a platinum sheet as the counter electrode at room temperature. After the anodization, the sample was immediately rinsed with deionized water and dried at room temperature. Then, it was annealed at 450 °C in air for 2 h at a heating rate of 5 °C min^{-1}.

Au NPs were loaded on the TiO_2 nanotube array film surface by a deposition–precipitation technique. Then, 8.8×10^{-3} M NaOH solution (15 mL) was added dropwise into a 2×10^{-3} M $HAuCl_4$ (15 mL) solution under vigorous stirring by a magnetic stirrer. The film sample was soaked in the above mixed solution in a Teflon-lined stainless steel autoclave at 140 °C for 1 h. Then the sample was taken out, washed with deionized water and dried in air.

ZnS capping layers were assembled on the Au/TiO_2 film surfaces by a SILAR method. The Au/TiO_2 film samples were alternately immersed in a 0.6 M $Zn(NO_3)_2$ ethanol solution and a 0.1 M Na_2S methanol solution for 1 min. Following each immersion, the films were rinsed successively with pure ethanol and deionized water to remove excess precursors, and dried at room temperature. Such an immersion cycle was repeated four times.

2.2 Characterization

The morphologies of the as-prepared films were characterized by a field-emission scanning electron microscope (SEM, Hitachi FE-SEM S4800) and a transmission electron microscope (TEM, JEOL JEM-2100) with an accelerating voltage of 200 kV. The chemical composition of the films was analyzed by energy dispersive X-ray (EDX) spectroscopy. The photoabsorption properties of the samples were recorded by a UV-Vis-NIR spectrophotometer (Varian, Cary 5000). The photoluminescence (PL) spectrum measurements were carried out by a fluorescence meter (F7000 Hitachi).

Chemical states of surface elements of the films were investigated by X-ray photoelectron spectroscopy (XPS, PHI Quantum 2000) with Al Kα as an exciting X-ray source. The spectra were calibrated with respect to the C1s line of adventitious carbon at 284.8 eV.

2.3 Photoelectrochemical measurements

Photoelectrochemical properties of the films were evaluated by a photoelectrochemical system, which is assembled by a potentiostat/galvanostat (model 263A, Princeton Applied Research, USA), a two phase lock-in amplifier (model 5210, Signal Recovery, USA) with a chopper (model ND-4, f = 34 Hz, China), and a 150 W xenon lamp with a SBP 300 monochromator. The as-prepared film served as a photoanode, and the photocurrent measurement was made by a three-electrode system consisting of a photoanode as the working electrode, a saturated calomel electrode (SCE) as the reference electrode and a platinum wire as the counter electrode. A mixed solution of 0.5 M KOH and 1 M CH_3OH was used as the electrolyte in the photoelectrochemical cell. The potential and electrochemical impedance spectroscopy (EIS) measurements were carried out by a home-made system including the photoelectrochemical cell and a corrosion cell with a 0.5 M NaCl solution. The photocathodic protection effects of the films were evaluated by measuring the potential variations of the 403SS coupled to the photoanodes with the different films in the presence and absence of white light illumination. EIS results were obtained by applying an AC voltage of 10 mV amplitude over the frequency range of 10^{-2} to 10^5 Hz under the illumination. The measured EIS data were fitted by Autolab EIS fitting software.

3 Results and discussion

3.1 Characterization of films

Fig. 1a shows a typical SEM image of a TiO_2 nanotube array film. It is clear that the resulting film consisted of self-organized nanotubes with an average external diameter of about 80 nm and a wall thickness of about 15 nm. Fig. 1b presents the SEM image of a Au/TiO_2 film and shows that the nanotube surfaces were decorated by Au NPs. After fabrication of a ZnS shell on the Au/TiO_2 film surface, we obtained a ZnS/Au/TiO_2 composite film as shown in Fig. 1c. From the high-magnification SEM image of Au NPs attached on the TiO_2 nanotubes as displayed in Fig. 1d, it can be seen that the Au NPs were uniformly distributed over the surface of the TiO_2 nanotube array film, without filling of the nanotubes. The SEM image of a cross section of the Au/TiO_2 film (Fig. 1e) shows that Au NP deposition occurred uniformly over the entire length of the nanotube walls, both on the interior and exterior surfaces of the nanotubes. To exactly reveal the structure of the Au/TiO_2 film, the sample was observed by TEM and the corresponding image is shown in Fig. 1f. The loaded Au NPs had an approximate spherical shape with 3–4 nm diameter. The Au NPs were all separated over the entire wall without any aggregation and were highly crystallized as evidenced from the well-resolved Au (111) crystalline lattices (0.24 nm).[34] After the consecutive

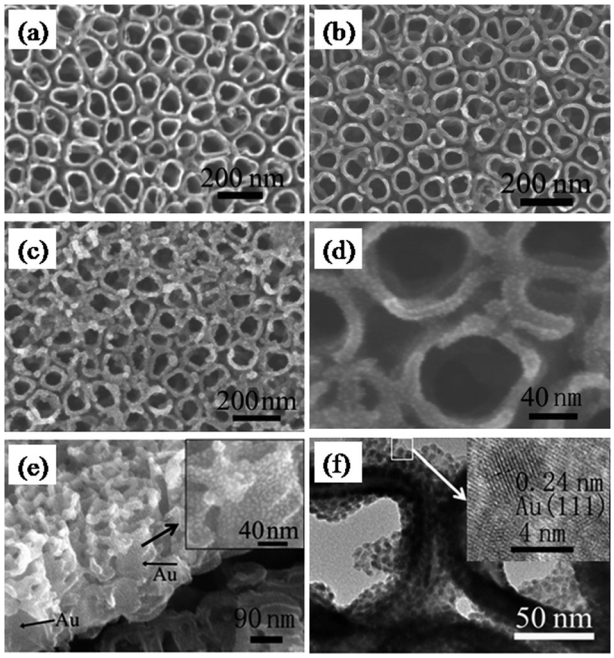

Fig. 1 SEM images of (a) the TiO_2 nanotube film, (b) the Au/TiO_2 film, and (c) the ZnS/Au/TiO_2 film. (d) High-magnification SEM image of the Au/TiO_2 film. (e) SEM image of the cross-section of the Au/TiO_2 film. (f) TEM image of the Au/TiO_2 film.

SILAR treatment, carried out four times by dipping the Au/TiO_2 film into a Zn^{2+} solution and a S^{2-} solution alternately, the wall thickness of the nanotubes showed a slight increase (Fig. 1c). As shown in Fig. 2, the EDX analysis of a ZnS/Au/TiO_2 composite nanotube film confirmed the presence of Ti, O, Au, Zn and S. Furthermore, the quantitative analysis of the EDX spectrum revealed that the molar ratio of Zn to S in the composite film was close to 1, indicating the stoichiometric formation of ZnS.

To further confirm the EDX analysis result, XPS analysis was also used to determine the chemical composition of the ZnS/Au/TiO_2 composite film (as shown in Fig. 3). Fig. 3a clearly shows that the surface layer of the ZnS/Au/TiO_2 film was composed of Ti, O, C, Au, Zn and S. In Fig. 3b, the Ti 2p peaks appearing at 458.7 and 464.4 eV were attributed to the Ti $2p_{3/2}$[35] and Ti $2p_{1/2}$[36] peaks, respectively, indicating that Ti existed in the form of Ti^{4+}.[37] As shown in Fig. 3c, two peaks existed at 530.86 and 532.39 eV in the O 1s XPS spectrum, which were attributed to the crystal lattice oxygen Ti–O in TiO_2[38,39] and hydroxyl groups O–H[40] in the sample surface layer, respectively. The quantitative analysis of the signals based on the peak areas gave the atomic ratio of O : Ti in the film as 2.04 : 1, which fits the stoichiometric number in TiO_2. The XPS spectrum of Au exhibited two peaks at 83.8 and 87.8 eV (Fig. 3d), originating from the Au $4f_{7/2}$ and $4f_{5/2}$ electrons of metallic gold, respectively.[41,42] The Au $4f_{7/2}$ (83.8 eV) peak shifted toward the lower value compared with the binding energy of bulk metallic gold (84.0 eV), which could be ascribed to the redistribution of electrons at the Au–TiO_2 contact interface.[43] Due to the difference in the work function between Au (5.27 eV)[44] and TiO_2 (4.1 eV),[45] it is reasonable that the electron transfer is facilitated from TiO_2 to Au NPs. This phenomenon might increase the valence charge density of Au atoms and reduce the binding energy of Au in the film. From Fig. 3e, it can be seen that the binding energy of Zn $2p_{3/2}$ was found at 1021.9 eV, which is consistent with measurements reported in the literature.[46] In Fig. 3f, the S 2p XPS spectrum could be fitted by two peaks located at 161.5 and 162.7 eV, which were ascribed to the core levels of S $2p_{3/2}$ and S $2p_{1/2}$, respectively.[47] The peak areas of the Zn and S cores were measured and yielded an atomic ratio of Zn to S as 1.07 : 1 for the composite film sample from the quantitative analysis by the sensitivity factors attached with the XPS instrument, which is in good agreement with the above-mentioned result of the EDX analysis.

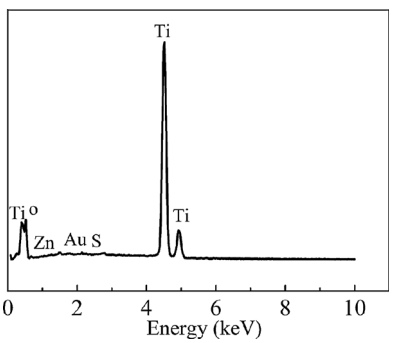

Fig. 2 EDX spectrum of the ZnS/Au/TiO_2 film.

Besides the crystallinity and microstructure, the surface and lattice defects (*e.g.* surface states, oxygen vacancies) play an important role in the photoactivity of the TiO_2 films. A PL emission spectrum is useful to disclose the efficiency of charge carrier trapping, migration and transfer, and to understand the lifetime of electron–hole pairs in semiconductor materials since PL emission mainly results from the recombination of free carriers.[48] For nanostructured materials, the PL spectra are related to the transfer behavior of the photo-induced electrons and holes so that they can be used to evaluate the recombination rate of charge carriers.[49] In general, the lower PL intensity indicates the lower recombination rate of electron–hole pairs under light irradiation. Usually, for anatase TiO_2 materials, there are three types of physical origins: self-trapped excitons, oxygen vacancies and surface states.[50] Fig. 4 shows the PL spectra of the prepared film samples. The peak at 481 nm resulted from the surface state as the existence of Ti^{4+}–OH.[48] It can be seen that the peak positions in the PL spectrum of the Au/TiO_2 film were in agreement with the pure TiO_2 film. However, the PL intensities were quite sensitive to Au modifying. The PL intensities of the Au/TiO_2 film sample were much lower than that of the TiO_2 sample, demonstrating that the Au NPs effectively suppressed the charge recombination in the Au/TiO_2 composite film.[51] Since the conduction band energy of TiO_2 (−0.29 V *vs.* NHE) is higher than the Fermi level of Au (+0.5 V *vs.* NHE), electrons were excited from the valence band to the conduction band of the TiO_2, and then migrated to Au NPs and accumulated to form a Schottky junction at the Au/TiO_2 interface.[20,21,52] Therefore, the direct recombination of

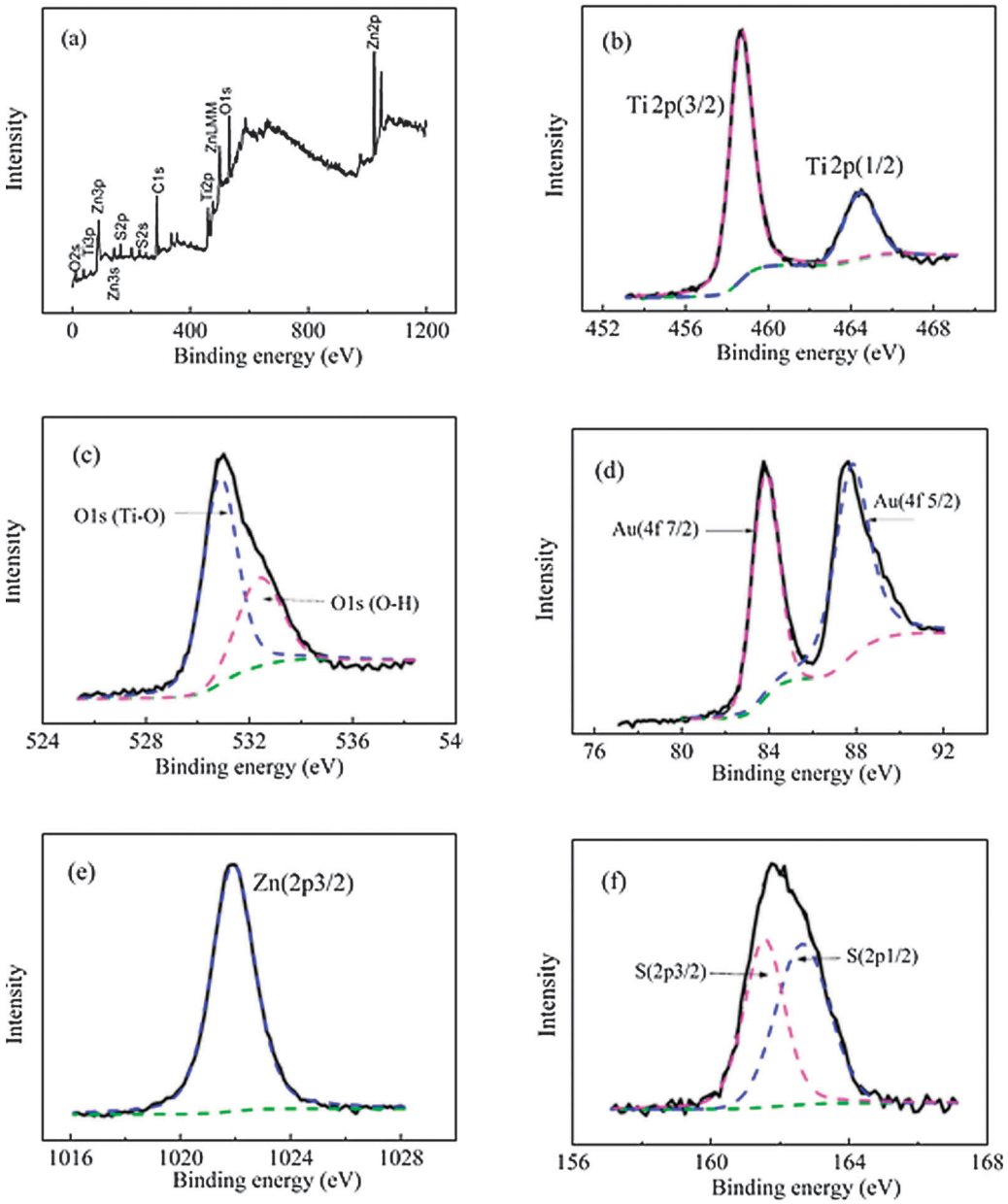

Fig. 3 XPS spectra of (a) the ZnS/Au/TiO_2 films, (b) Ti 2p, (c) O 1s, (d) Au 4f, (e) Zn 2p and (f) S 2p.

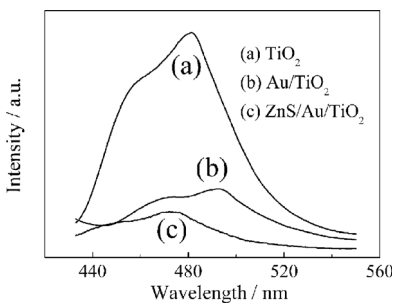

Fig. 4 PL spectra of the TiO_2 film, and the Au/TiO_2 and ZnS/Au/TiO_2 composite films.

electrons and holes could be prevented. This would facilitate the electron transfer and improve electron–hole separation. It is well known that the PL emission results from the recombination of photo-generated electrons and holes. Consequently, it is reasonable that the PL intensities of the Au/TiO_2 film were much lower than that of the TiO_2 film. This result suggests that Au NPs on TiO_2 surface are able to extract electrons from the conduction band of TiO_2 and thus prevent charge carrier recombination. When a ZnS shell was prepared onto the Au/TiO_2 film surface, the reduction of PL intensities and no PL peaks of ZnS were observed (shown in Fig. 4c), indicating that the finally deposited ZnS layer hardly participated in harvesting light but played a role in improving charge separation.

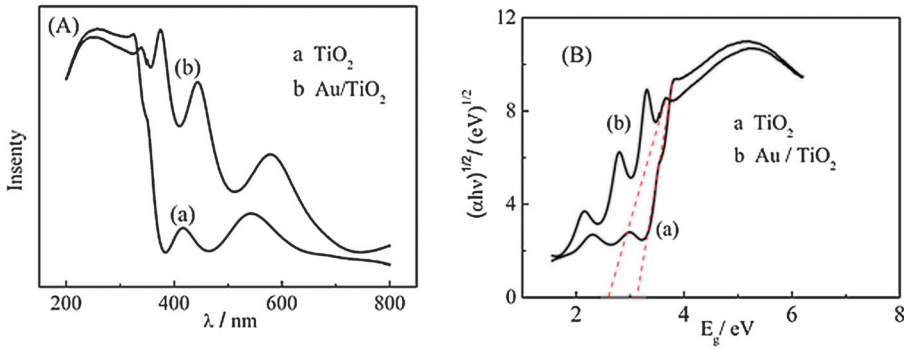

Fig. 5 (A) The UV-vis absorption spectra and (B) the plots of $(\alpha h\nu)^{1/\eta}$ *versus* $h\nu$ for a TiO_2 film and a Au/TiO_2 film.

To investigate the light absorption properties of the synthesized TiO_2 films and the effect of Au NPs on the UV-vis light response, the UV-vis absorption spectra of the pure TiO_2 and Au/TiO_2 films were measured and displayed in Fig. 5A. It can be observed that considerable UV absorption appeared from 200 to 400 nm for the two films, which was primarily ascribed to the electron promotion of TiO_2 from the valence band to the conduction band.[53] Compared with the pure TiO_2 film, the absorption edge of the Au/TiO_2 film was obviously shifted to the visible light region. This could be confirmed by roughly estimating the band gap as shown in Fig. 5B. The optical band gap energy can be estimated by the following equation for a semiconductor:[54]

$$\alpha h\nu = A(h\nu - E_g)^{\eta} \quad (1)$$

where α is the optical adsorption coefficient, which represents the absorption ability of a material for a certain wavelength; h is the Planck constant; ν is the frequency of light; A is a constant, which depends on temperature, photo energy and phonon energy; E_g is the band gap; the exponent η is a characteristic of the type of electrons transition process (η = 1/2 for a direct allowed transition, η = 2 for an indirect allowed transition process).[54] Assuming the Au/TiO_2 composite film to be an indirect semiconductor, as is TiO_2, the band gap can be determined by extrapolating the liner portion of the plot of $(\alpha h\nu)^{1/2}$ *versus* $h\nu$ to $\alpha = 0$.[55] The estimated band gap values of TiO_2 and Au/TiO_2 films were approximately 3.14 and 2.53 eV, respectively. It is evident that the Au NPs loading induced a red shift for the optical absorption (shown in Fig. 5A). As Au NPs were distributed on the surface of the TiO_2 film to develop a Schottky junction, the interaction of Au and TiO_2 might introduce the intra-gap energy levels inside the band gap of TiO_2, which was responsible for the shift of the Au/TiO_2 film absorption edge.[24] Therefore, it could be concluded that the Au NPs had a crucial effect on the optical properties of the Au/TiO_2 composite film.

Incident photon-to-current conversion efficiency (IPCE) is also referred to as external quantum efficiency (EQE), which is the ratio of electrons collected per incident photon. Therefore, IPCE is a valuable parameter to characterize the photo-conversion property, which can be expressed by the following equation:[56]

$$\mathrm{IPCE} = 1240\frac{I}{\lambda P_{\mathrm{in}}} \quad (2)$$

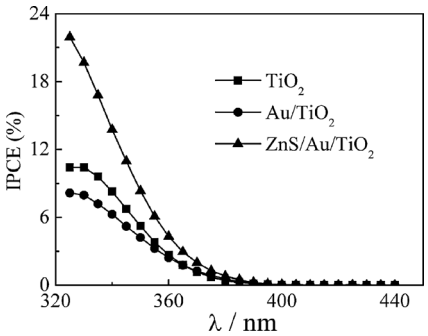

Fig. 6 IPCE spectra of the different films.

where I is the photocurrent density at a specific wavelength, λ is the wavelength of incident light, and P_{in} is the intensity of the light at a specific wavelength. In this work, IPCE measurements were performed to understand the photoresponse performance of the prepared films under illumination across different wavelengths. Fig. 6 shows the IPCE results for the different films. It can be observed that the pure TiO_2 film exhibited the maximum IPCE of 10% at 325 nm, while the Au/TiO_2 film showed the maximum IPCE of 8%, indicating that Au NPs did not improve the value of the IPCE as suggested by Liu *et al.*[57] The reduction of IPCE observed in the Au/TiO_2 film might arise due to two reasons. First, with Au NPs acting as a sink for photogenerated electrons, it is likely that the electrons stored in Au NPs were shielded by the cations (Na^+).[58,59] Second, the electron scavenging by O_2 in the electrolyte could also partially contribute to the reduction of IPCE.[58] Although Au NPs could effectively inhibit the recombination of electron–hole pairs, most of the electrons on the surface of Au NPs reacted with the electrolyte, and the electrons trapped by the Au NPs could not effectively improve the photocurrent. Consequently, the IPCE of the Au/TiO_2 film was lower.

Although the deposition of Au NPs reduced the IPCE of Au/TiO_2 film, it can be clearly observed that the IPCE of the $ZnS/Au/TiO_2$ film was significantly enhanced. A thin ZnS shell formed by a SILAR process could prevent the electron leakage from the Au NP surface due to its higher conduction band.[60,61] This result is consistent with the study by Mora-Sero *et al.* on recombination in quantum dot sensitized solar cells.[62] The ZnS layer acted as the energy barrier between the Au NPs and the

electrolyte, which could reduce the recombination of electrons from the surface of Au NPs with the electrolyte (electrons capture agent). This increased the lifetime of electrons and leaded to the enhanced electron injection efficiency. Consequently, a much higher IPCE could be obtained because the leakage of electrons from Au NPs surface was decreased.

3.2 Photoelectrochemical properties

Cathodic protection is the technique of reducing the metal corrosion rate by shifting the corrosion potential of the metal electrode toward a lower potential by applying an external electromotive force. Therefore, we can measure the potential of a metal coupled with a TiO_2 film or its composite film to evaluate the photoelectrochemical properties or photocathodic protection effect of the film. Fig. 7 shows the potential response of 403SS in a 0.5 M NaCl solution coupled to the different films as photoanodes under intermittent illumination. It can be clearly observed that the potential abruptly decreases or increases as the light was turned on or off. Under irradiation, the potential of 403SS shifted negatively to lower potentials and then to the relatively stable potentials owing to the balance state between creation and depletion of photogenerated electrons. When the light was turned off, the potential increased promptly due to fast charge recombination. These results indicated that the prepared films could exhibit a photocathodic protection effect on the steel, but the photoelectrochemical effect of the $ZnS/Au/TiO_2$ composite film was more significant than that of the pure TiO_2 film. When illuminated, the composite film could immediately shift the potential of the coupled 403SS from about 20 mV (the corrosion potential) to about −380 mV (namely the photopotential) as shown in Fig. 7b, indicating that a large number of photoelectrons were transferred to the steel so as to lead to the cathodic polarization of 403SS, and that the composite film exhibited the higher generation separation and transfer efficiency of photogenerated electrons. When the composite film continued to be illuminated after a break, the 403SS potential again dropped to about −380 mV, showing that the composite film exhibited substantial activity and stability. Significantly, when illumination was stopped, the steel potential remained about −125 mV lower than the corrosion potential, indicating

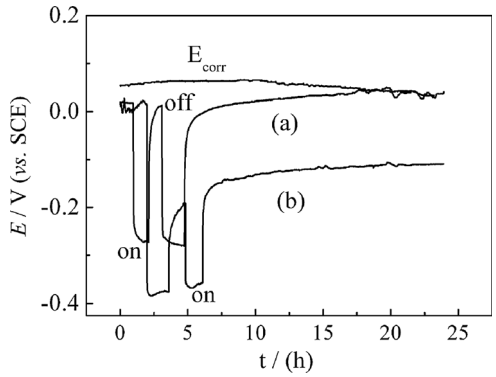

Fig. 7 Time evolution of the potential of 403SS coupled to different film photoanodes under illumination and dark conditions. (a) TiO_2, (b) $ZnS/Au/TiO_2$.

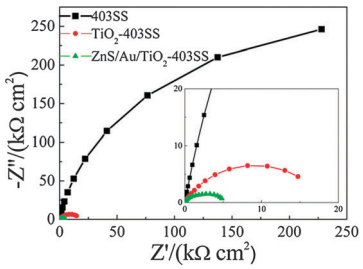

Fig. 8 EIS results for 403SS in a 0.5 M NaCl solution under different conditions.

that the composite film still provided a certain cathodic protection for the steel in the dark. The above-mentioned results indicated that the $ZnS/Au/TiO_2$ film had excellent photoelctrochemical properties, which is consistent with the IPCE measurement on the same film.

EIS analysis can provide electrochemical information at the metal–solution interface, thus it is beneficial to study the corrosion behavior of metals.[63] The EIS spectra and fitted results of 403SS coupled and uncoupled with different samples are shown in Fig. 8. In order to give quantitative support to the EIS results, impedance parameters were obtained using Autolab software with the equivalent circuit (as shown in Fig. 9), where R_s is the solution resistance, R_{ct} is the charge-transfer resistance, and CPE is the constant phase elements modeling the capacitance of the double-layer. The impedance of CPE is defined as follows:

$$Z_{CPE} = Y_0^{-1}(j\omega)^{-n} \quad (3)$$

where Y_0 represents the modulus, ω is the angular frequency, and n is the coefficient of diffusion.[64,65]

According to the fitting data from the EIS results, the value of R_{ct} was 579 kΩ cm^2 for the uncoupled 403SS. Under light illumination, the impedance arc radius of the 403SS coupled to the film photoanodes was much smaller than the uncoupled 403SS electrode, indicating that a large number of photogenerated electrons was transferred from the photoanode to the steel per unit time and made the cathodic current densities for the steel increase. Furthermore, the arc radius of the 403SS coupled to the $ZnS/Au/TiO_2$ electrode was obviously smaller than that coupled to the TiO_2 electrode. According to the fitting results, the R_{ct} values were 3.48 and 17.1 kΩ cm^2 for the 403SS coupled to the $ZnS/Au/TiO_2$ and the TiO_2 electrodes, respectively, which demonstrated that the $ZnS/Au/TiO_2$ composite film exhibited a greater separation efficiency of photogenerated electron–hole pairs and faster charge transfer than the pure TiO_2 film. As discussed above, the $ZnS/Au/TiO_2$ composite film

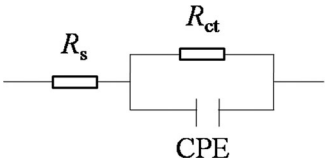

Fig. 9 Simulating equivalent circuit for the EIS results.

could provide a better photocathodic protection effect for 403SS than that of the pure TiO_2 film.

4 Conclusions

We have fabricated a ZnS/Au/TiO_2 composite nanotube array film modified by Au NPs and a ZnS shell. Au NPs could be loaded on the surface of the TiO_2 nanotube film in the form of metallic Au. The visible light absorption intensity of the composite film was enhanced because Au NPs were able to trap photogenerated electrons and improve the electron–hole pair lifetime. The ZnS/Au/TiO_2 composite film as a photoanode could provide a more effective photocathodic protection effect than the pure TiO_2 film. When we coupled the 403SS in a 0.5 M NaCl solution to the ZnS/Au/TiO_2 film photoanode, its potential decreased by 400 mV under white light illumination, and kept at the lower values than the corrosion potential under dark conditions. Furthermore, the charge transfer resistance of 403SS coupled with the composite film photoelectrode became distinctly smaller under illumination, indicating that a large number of photogenerated electrons were transferred to the steel from the photoelectrode, providing cathodic polarization.

Acknowledgements

This work was supported by the National Natural Science Foundation of China (Nos. 21173177, 21073151, and 21021002). We thank Dr K. Tan for helpful conversations.

References

1 S. Iijima, *Nature*, 1991, **354**, 56.
2 A. M. Morales and C. M. Lieber, *Science*, 1998, **279**, 208.
3 M. He, J. Ge, Z. Q. Lin, X. H. Feng, H. B. Lu, Y. L. Yang and F. Qiu, *Energy Environ. Sci.*, 2012, **5**, 8351.
4 X. K. Xin, J. Wang, W. Han, M. D. Ye and Z. Q. Lin, *Nanoscale*, 2012, **4**, 964.
5 M. D. Ye, J. J. Gong, Y. K. Lai, C. J. Lin and Z. Q. Lin, *J. Am. Chem. Soc.*, 2012, **134**, 15720.
6 Y. H. Jang, X. K. Xin, M. Byun, Y. J. Jang, Z. Q. Lin and D. H. Kim, *Nano Lett.*, 2012, **12**, 479.
7 M. He, J. H. Jung, F. Qiu and Z. Q. Lin, *J. Mater. Chem.*, 2012, **22**, 24254.
8 X. K. Xin, M. Scheiner, M. D. Ye and Z. Q. Lin, *Langmuir*, 2011, **27**, 14594.
9 S. Sreekantan, R. Hazan and Z. Lockman, *Thin Solid Films*, 2009, **518**, 16.
10 H. F. Zhuang, C. J. Lin, Y. K. Lai, L. Sun and J. Li, *Environ. Sci. Technol.*, 2007, **41**, 4735.
11 G. K. Mor, K. Shankar, M. Paulose, O. K. Varghese and C. A. Grimes, *Nano Lett.*, 2005, **5**, 191.
12 M. Paulose, G. K. Mor, O. K. Varghese, K. Shankar and C. A. Grimes, *J. Photochem. Photobiol., A*, 2006, **178**, 8.
13 K. Shankar, G. K. Mor, H. E. Prakasam, O. K. Varghese and C. A. Grimes, *Langmuir*, 2007, **23**, 12445.
14 A. Subramanian and H. W. Wang, *Appl. Surf. Sci.*, 2012, **258**, 6479.
15 S. C. Roy, M. Paulose and C. A. Grimes, *Biomaterials*, 2007, **28**, 4667.
16 K. C. Popat, L. Leoni, C. A. Grimes and T. A. Desai, *Biomaterials*, 2007, **28**, 3188.
17 J. Zhang, R. G. Du, Z. Q. Lin, Y. F. Zhu, Y. Guo, H. Q. Qi, L. Xu and C. J. Lin, *Electrochim. Acta*, 2012, **83**, 59.
18 O. K. Varghese, D. W. Gong, M. Paulose, K. G. Ong, E. C. Dickey and C. A. Grimes, *Adv. Mater.*, 2003, **15**, 624.
19 Q. Wang, Y. Z. Pan, S. S. Huang, S. T. Ren, P. Li and J. J. Li, *Nanotechnology*, 2011, **22**, 025501.
20 V. Iliev, D. Tomova, L. Bilyarska, A. Eliyas and L. Petrov, *Appl. Catal., B*, 2006, **63**, 266.
21 V. Subramanian, E. E. Wolf and P. V. Kamat, *J. Am. Chem. Soc.*, 2004, **126**, 4943.
22 L. Armelao, D. Barreca, G. Bottaro, A. Gasparotto, E. Tondello, M. Ferroni and S. Polizzi, *Chem. Mater.*, 2004, **16**, 3331.
23 A. A. Ismail, D. W. Bahnemann, I. Bannat and M. Wark, *J. Phys. Chem. C*, 2009, **113**, 7429.
24 F. M. Cui, Z. L. Hua, C. Y. Wei, J. Q. Li, Z. Gao and J. L. Shi, *J. Mater. Chem.*, 2009, **19**, 7632.
25 S. Chen, M. Malig, M. Tian and A. C. Chen, *J. Phys. Chem. C*, 2012, **116**, 3298.
26 M. G. Hosseini, M. M. Momeni and M. Faraji, *Electroanalysis*, 2011, **23**, 1654.
27 Q. Zhao, M. Li, J. Y. Chu, T. S. Jiang and H. B. Yin, *Appl. Surf. Sci.*, 2009, **255**, 3773.
28 I. Paramasivalm, J. M. Macak and P. Schmuki, *Electrochem. Commun.*, 2008, **10**, 71.
29 F. Xiao, *J. Mater. Chem.*, 2012, **22**, 7819.
30 M. V. Dozzi, L. Prati, P. Canton and E. Selli, *Phys. Chem. Chem. Phys.*, 2009, **11**, 7171.
31 P. Fu and P. Zhang, *Thin Solid Films*, 2011, **519**, 3480.
32 J. F. Reber and K. Meier, *J. Phys. Chem.*, 1984, **88**, 5903.
33 P. V. Kamat and B. Shanghavi, *J. Phys. Chem. B*, 1997, **101**, 7675.
34 P. Fu and P. Zhang, *Appl. Catal., B*, 2010, **96**, 176.
35 J. Wang, D. N. Tafen, J. P. Lewis, Z. L. Hong, A. Manivannan, M. J. Zhi, M. Li and N. Q. Wu, *J. Am. Chem. Soc.*, 2009, **131**, 12290.
36 L. J. Chen, F. Chen, Y. F. Shi and J. L. Zhang, *J. Phys. Chem. C*, 2012, **116**, 8579.
37 T. Kuho and A. Nakahira, *J. Phys. Chem. C*, 2008, **112**, 1658.
38 R. P. Antony, T. Mathews, S. Dash, A. K. Tyagi and B. Raj, *Mater. Chem. Phys.*, 2012, **132**, 957.
39 L. V. Taveira, J. M. Macak, H. Tsuchiya, L. F. P. Dick and P. Schmuki, *J. Electrochem. Soc.*, 2005, **152**, B405.
40 H. M. Liu, W. S. Yang, Y. Ma, Y. Cao, J. N. Yao, J. Zhang and T. D. Hu, *Langmuir*, 2003, **19**, 3001.
41 Q. Fu, H. Saltsburg and M. Flytzani-Stephanopoulos, *Science*, 2003, **301**, 935.
42 Y. Lu, H. T. Yu, S. Chen, X. Quan and H. M. Zhao, *Environ. Sci. Technol.*, 2012, **46**, 1724.

43 J. Fang, S. W. Cao, Z. Wang, M. M. Shahjamali, S. C. J. Loo, J. Barber and C. Xue, *Int. J. Hydrogen Energy*, 2012, **37**, 17853.
44 C. D. Zangmeister, L. B. Picraux, R. D. van Zee, Y. X. Yao and J. M. Tour, *Chem. Phys. Lett.*, 2007, **442**, 390.
45 T. Ioannides and X. E. Verykios, *J. Catal.*, 1996, **161**, 560.
46 S. W. Lu and H. K. Schmidt, *Mater. Res. Bull.*, 2008, **43**, 583.
47 J. Yang, J. J. Peng, R. X. Zou, F. Peng, H. J. Wang, H. Yu and J. Y. Lee, *Nanotechnology*, 2008, **19**, 255603.
48 K. Nagaveni, M. S. Hegde and G. Madras, *J. Phys. Chem. B*, 2004, **108**, 20204.
49 F. B. Li and X. Z. Li, *Appl. Catal., A*, 2002, **228**, 15.
50 J. Zhang, X. G. Chen, Y. D. Li, Y. W. Shen, Z. G. Hu and J. H. Chu, *Phys. Chem. Chem. Phys.*, 2011, **13**, 13096.
51 X. Wang, M. Blackford, K. Prince and R. A. Caruso, *ACS Appl. Mater. Interfaces*, 2012, **4**, 476.
52 E. Bae and W. Choi, *Environ. Sci. Technol.*, 2003, **37**, 147.
53 N. Zhang, S. Liu, X. Fu and Y. J. Xu, *J. Phys. Chem. C*, 2011, **115**, 9136.
54 R. Pandiyan, V. Micheli, D. Ristic, R. Bartali, G. Pepponi, M. Barozzi, G. Gottardi, M. Ferrari and N. Laidani, *J. Mater. Chem.*, 2012, **22**, 22424.
55 N. Naseri, M. Amiri and A. Z. Moshfegh, *J. Phys. D: Appl. Phys.*, 2010, **43**, 105405.
56 S. Hoang, S. Guo, N. T. Hahn, A. J. Bard and C. B. Mullins, *Nano Lett.*, 2012, **12**, 26.
57 L. Liu, G. Wang, Y. Li, Y. Li and J. Z. Zhang, *Nano Res.*, 2010, **4**, 249.
58 V. Subramanian, E. Wolf and P. V. Kamat, *J. Phys. Chem. B*, 2001, **105**, 11439.
59 M. Jakob, H. Levanon and P. V. Kamat, *Nano Lett.*, 2003, **3**, 353.
60 M. H. Jung and M. G. Kang, *J. Mater. Chem.*, 2011, **21**, 2694.
61 Z. X. Li, Y. L. Xie, H. Xu, T. M. Wang, Z. G. Xu and H. L. Zhang, *J. Photochem. Photobiol., A*, 2011, **224**, 25.
62 I. Mora-Sero, S. Gimenez, F. Fabregat-Santiago, R. Gomez, Q. Shen, T. Toyoda and J. Bisquert, *Acc. Chem. Res.*, 2009, **42**, 1848.
63 W. A. Badawy and F. M. Al-Kharafi, *Electrochim. Acta*, 1998, **44**, 693.
64 W. Chen, R. G. Du, C. Q. Ye, Y. F. Zhu and C. J. Lin, *Electrochim. Acta*, 2010, **55**, 5677.
65 P. Wang, D. Zhang and R. Qiu, *Corros. Sci.*, 2012, **54**, 77.

